J Therm Anal Calorim (2014) 115:471–477
DOI 10.1007/s10973-013-3281-2

Synthesis and characterization of manganese–zinc ferrite obtained by thermal decomposition from organic precursors

Irena Szczygieł · Katarzyna Winiarska

Received: 18 March 2013 / Accepted: 4 June 2013 / Published online: 30 June 2013
© The Author(s) 2013. This article is published with open access at Springerlink.com

Abstract Mn–Zn ferrites were obtained by the sol–gel autocombustion methods. The effect of the precursor used in the sol–gel autocombustion synthesis on the ferrite's microstructure was examined. The as-obtained powders were characterized by XRD, FTIR, SEM, and TG/DTA. All ferrite powders obtained from different organic precursors, after gel autocombustion, were pure spinel phase, without secondary phases. The average crystallite size, estimated from Scherrer equation, was the smallest for ferrite obtained from a mixture of fuels/precursors (citric acid and EDTA). This ferrite powder has sponge-like microstructure with large pores, but it is less agglomerated than the material obtained from glycine as the fuel.

Keywords Mn–Zn ferrite · Nanomaterials · Autocombustion · TG/DTA

Introduction

Nanopowders, especially magnetic ones, because of the particular size of their grains, show many features setting them apart from bulk materials and, therefore, can find new areas of applications. Owing to their developed specific surface and high surface energy they can be used as catalysts [1–3] or gas sensors [4]. Nanoferrites with below-critical grain size at room temperature are characterized by superparamagnetism, low Curie temperature, and high magnetic flux density. These characteristics have enabled the use of nanosized magnetic materials in biomedicine (e.g., as bioseparators), drug delivery systems, medical diagnostics, and cancer thermotherapy [5–7]. Due to the new applications of ferrites ways of synthesizing them, other than the ceramic method, such as the sol–gel [8, 9], the precipitation [10, 11], the mechanochemical [12, 13], the hydrothermal [14, 15], the combustion [16–20], and the microemulsion methods [21, 22], are being widely investigated. The unquestionable advantages of the above methods are: the mixing together of the reagents at the molecular level, energy efficiency, the fact that only one process stage is required, and the absence of secondary pollution or material loss. Chemical methods are used to synthesize highly homogenous nanocrystalline ferrite with developed specific surface area. However, as in the case of the combustion method, unstable powders, forming hard agglomerates, can be obtained [23]. Because of their unstable character, foreign nonmagnetic phases (e.g., hematite: Fe_2O_3) may occur as a result of the further thermal treatment [24, 25].

In recent years many reports on synthesizing Mn–Zn powders by combustion methods have been published, but the formation of hard agglomerates has rarely been mentioned. As part of the present study, ferrites with the composition $Mn_{0.6}Zn_{0.4}Fe_2O_4$ were synthesized through the sol–gel autocombustion method using various organic precursors. The influence of the precursor on the quality of the obtained products was also determined. We also reported a novel way to produce soft agglomerated Mn–Zn ferrite powders after sol–gel autocombustion synthesis. Such a method, in which a mixture of complexing fuels and the additional drying of the gel were used, was previously described for other compounds [26].

I. Szczygieł · K. Winiarska (✉)
Department of Inorganic Chemistry, Faculty of Engineering and Economics, Wrocław University of Economics, Komandorska 118/120, 53-345 Wrocław, Poland
e-mail: katarzyna.winiarska@ue.wroc.pl

Experimental

Mn–Zn ferrite preparation

Manganese–zinc ferrite powders with the composition $Mn_{0.6}Zn_{0.4}Fe_2O_4$ were prepared by the sol–gel autocombustion method. The stechiometric amounts of manganese nitrate [$Mn(NO_3)_2{\cdot}4H_2O$], zinc nitrate [$Zn(NO_3)_2{\cdot}6H_2O$], and iron nitrate [$Fe(NO_3)_3{\cdot}9H_2O$] were dissolved in distilled water. Then appropriate amount of fuel (glycine, citric acid, or CA and EDTA mixture) was added to nitrate solution with continuous stirring with a magnetic agitator. The molar ratio of the fuel to the total amount of metal ions (F/M) was set at 2. Whereas the oxidant to fuel (O/F) molar ratio amounted to 5; therefore, the mixture was supplemented with an appropriate quantity of concentrated nitric acid (*V*). In case citric acid and citric acid (CA) with EDTA mixture were used as the fuel of autocombustion process, the final pH was adopted as 7, because above pH = 6 citric acid occurs mainly in the form of $HCit^{2-}$ and Cit^{3-} ions, which favors better complexing of the metal ions [27]. The pH was adjusted by adding 25 vol% ammonia solution. The brown sols were heated until the gels have been formed. When citric acid or glycine was the fuel, samples were heated until the gel spontaneously combusted. Gel prepared from a mixture of CA and EDTA was additionally dried at 120 °C and then rapidly heated to initiate the spontaneous combustion. Finally, the loose ferrite powders were obtained.

Mn–Zn ferrite characterization

Powder X-ray diffraction measurements (XRD) at room temperature were performed with a Siemens D 5000 diffractometer using CuKα-radiation (scanning rate of 3–6°min^{-1} and an angle range of 2θ: 25°–60°). The average crystallite size d_{XRD} was estimated from XRD line broadening using the Scherrer equation: $d_{XRD} = K\lambda/(B - B_0)\cos\theta$, where d_{XRD} is the average crystallite size in the direction perpendicular to the (*hkl*) plane of reflexes in nm, K = 0.9 is a Scherrer constant (as proposed by Klug et al. [28]), $\lambda = 0.154$ nm is the X-ray wavelength used in the measurement, B and B_0 are the full-width at half-maximum (FWHM) of the diffraction peak at angle θ and the corrected instrumental broadening (in rad), respectively. The (311) peak was chosen for calculations as the most suitable for crystallite size determination.

Thermal analysis (TG/DTA) was carried out with a derivatograph type 3427 (MOM, Hungary), from 20 to 1300 °C under air (heating rate: 7.5 °C min^{-1}, reference material: α-alumina, platinum crucibles, Pt/PtRh10 thermocouple).

The Fourier transform infrared spectra were recorded on a PERKIN-ELMER SYSTEM 2000 FTIR spectrophotometer in the range of wavenumbers 400–4000 cm^{-1} using KBr-pressed pellets.

The morphology of the ferrite powders was investigated by a scanning electron microscope (JOEL JSM-5800LV and FEI Quanta^{TM}250). The compositional analysis of different areas of the samples was carried out by an energy dispresion X-ray (EDAX) analyzer.

Results and discussion

In the combustion synthesis, besides the target product (Mn–Zn ferrite), gases in the most stable form, i.e., CO_2, H_2O, and N_2, are produced as gel is being combusted. Based on the above assumption, Jain et al. [29] proposed thermochemical calculations for the condensed fuel-oxidizer mixtures. Carbon and hydrogen with a valence of 4^+ and 1^+, respectively, are regarded as reducing agents, oxygen with a valence of 2^- is regarded as an oxidizing agent and the valence of nitrogen amounts to zero. Using these principles, the oxidizing valences of the oxidizers and the fuels were calculated (Table 1). The stoichiometric redox reaction for the systems in which O/F = 5 and F/M = 2 might proceed according to the proposed equations:

Fuel: glycine

$$0.6Mn(NO_3)_2 + 0.4Zn(NO_3)_2 + 2Fe(NO_3)_{3(s)} + 22HNO_{3(l)} + 6NH_2CH_2COOH_{(l)} \rightarrow Mn_xZn_{1-x}Fe_2O_{4(c)} + 12CO_{2(g)} + 18N_{2(g)} + 26H_2O_{(g)} + 24O_{2(g)} \quad (1)$$

Table 1 The oxidizing valences of the oxidizers and fuels at sol–gel autocombustion process

Compound	Derivation	Valency oxidizing (−), reducing (+)
Oxidizers		
$M_I(NO_3)_2$, M_I = Zn, Mn	$2 + 2{\cdot}[0 + 3{\cdot}(-2)]$	−10
$M_{II}(NO_3)_3$, M_{II} = Fe	$3 + 3{\cdot}[0 + 3{\cdot}(-2)]$	−15
HNO_3	$+1 + 0 + 3{\cdot}(-2)$	−5
Fuels		
Glycine ($C_2H_5NO_2$)	$2{\cdot}(+4) + 5{\cdot}(+1) + 0 + 2{\cdot}(-2)$	9
Citric acid ($C_6H_8O_7$)	$6{\cdot}(+4) + 8{\cdot}(+1) + 7{\cdot}(-2)$	18
EDTA ($C_{10}H_{16}N_2O_8$)	$10{\cdot}(+4) + 16{\cdot}(+1) + 0 + 8{\cdot}(-2)$	40
NH_4OH	$0 + 4{\cdot}(+1) + (-2) + 1$	3

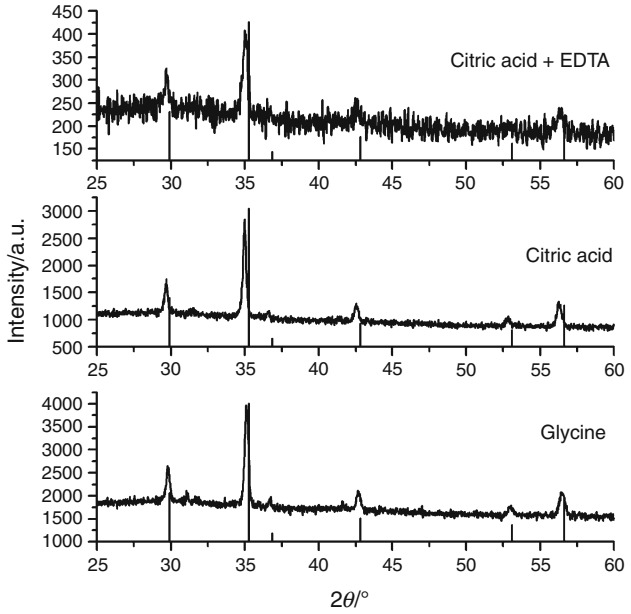

Fig. 1 XRD patterns of Mn–Zn ferrite powders after autocombustion prepared from different fuels

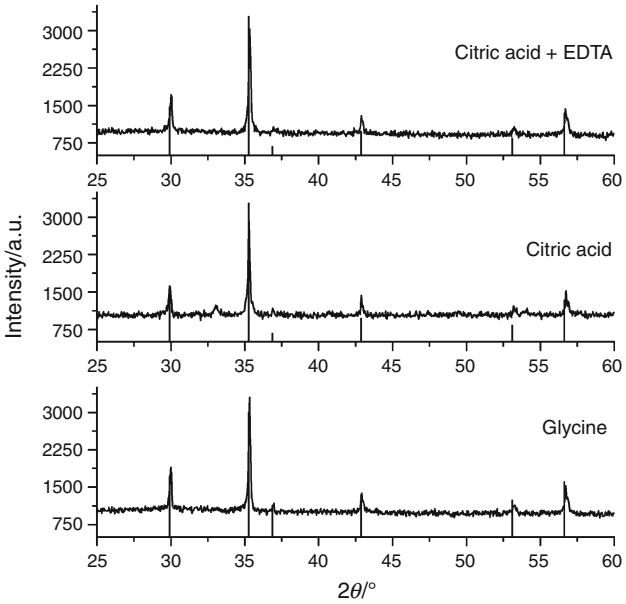

Fig. 2 XRD patterns of Mn–Zn ferrite powders after TG/DTA analysis

Fuel: citric acid

$$0.6Mn(NO_3)_2 + 0.4Zn(NO_3)_2 + 2Fe(NO_3)_{3(s)} + 22HNO_{3(l)} + 6C_6H_8O_{7(l)} + 2NH_4OH_{(l)} \rightarrow Mn_xZn_{1-x}Fe_2O_{4(c)} + 36CO_{2(g)} + 16N_{2(g)} + 40H_2O_{(g)} + 9O_{2(g)} \quad (2)$$

Fuel: citric acid + EDTA

$$0.6Mn(NO_3)_2 + 0.4Zn(NO_3)_2 + 2Fe(NO_3)_{3(s)} + 22HNO_{3(l)} + 6\left[C_6H_8O_{7(l)} + C_{10}H_{16}N_2O_8\right] + 2NH_4OH_{(l)} + 51O_{2(g)} \rightarrow Mn_xZn_{1-x}Fe_2O_{4(c)} + 96CO_{2(g)} + 22\,N_{2(g)} + 88H_2O_{(g)} \quad (3)$$

In the proposed synthesis conditions the combustion reaction had a mixed character. Both volumetric combustion and self-propagating combustion occurred, because of the reaction wave propagated over the entire volume and the combustion, which lasted from a few to several seconds. Thus the combustion in the above systems can be defined as volumetric-self-propagating combustion [30].

An analysis of the XRD patterns, shown in Fig. 1, indicates that ferrite powder with a spinel structure forms as a result of gel combustion. The peaks in the X-ray database standard (JCPDS-ICDD 22-1012) are slightly shifted relative to the peaks originating from the synthesized phases, which may be due to the formation of a mixture of ferrites in metastable form after gel combustion. Earlier, this phenomenon was observed by Angermann et al. [25] for low-temperature ferrite synthesis. During the synthesis manganese ferrite with a large number of oxygen

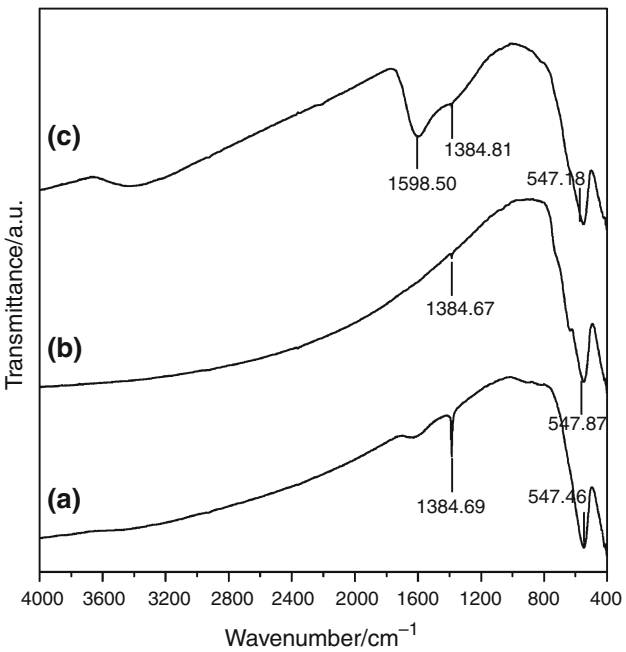

Fig. 3 FTIR spectra of Mn–Zn ferrite powders after autocombustion prepared from different fuels: (*a*) glycine, (*b*) citric acid, and (*c*) citric acid and EDTA

vacancies and Mn–Zn ferrite rich in zinc were obtained. When the powders are heated, the defective Mn ferrite precipitates in the form of hematite and bixbyite, which co-occur with ferrite having a spinel structure [25]. At high temperatures the foreign phases again get incorporated into the crystal lattice of the spinel ferrite, which is reflected in the XRD pattern (Fig. 2) of the powders after

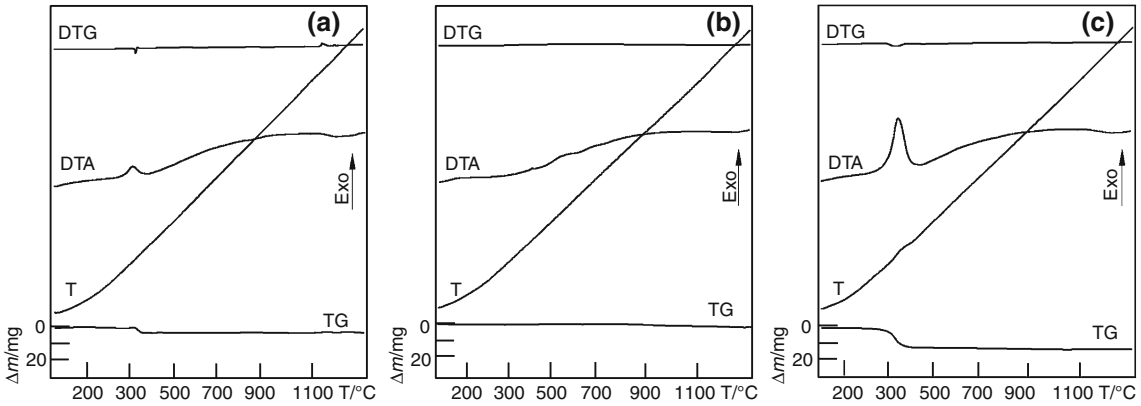

Fig. 4 The T/TG/DTA curves of samples prepared from (**a**) glycine, (**b**) citric acid, and (**c**) citric acid and EDTA

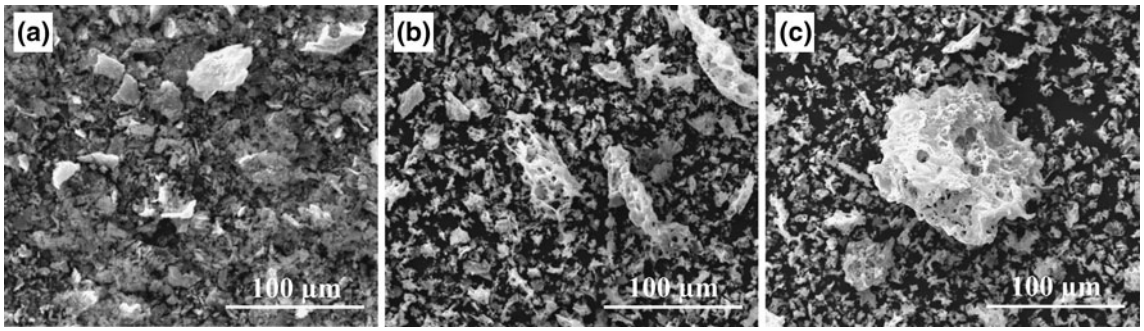

Fig. 5 SEM images of ferrite powders obtained from different fuels: (**a**) glycine, (**b**) citric acid, and (**c**) citric acid and EDTA. Magnification: ×1000

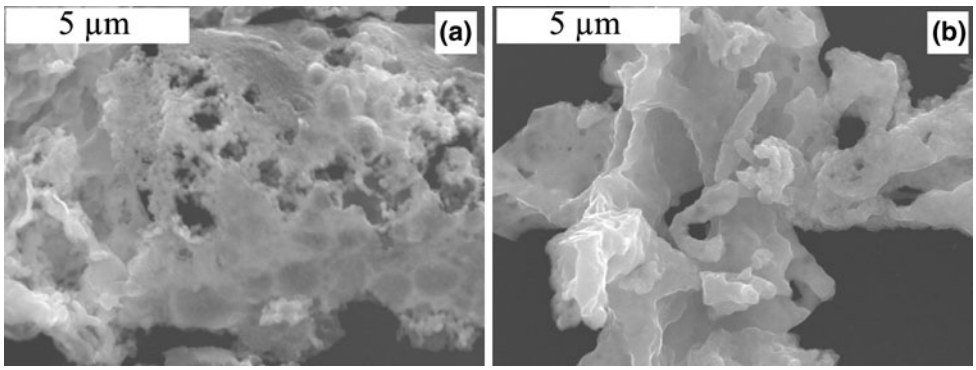

Fig. 6 Microstructure (larger magnification) of ferrite powders prepared from (**a**) glycine, (**b**) citric acid and EDTA precursors. Magnification: ×10000

the TG/DTA analysis. Then all the peaks originating from the spinel phase coincide with the standard spinel peaks (JCPDS-ICDD 22-1012). The average crystallites size of the synthesized powders, calculated from the Scherrer equation for peak (311) amounts to 50.2, 69.1, and 40.0 nm for the tests with glycine, citric acid, and a mixture of CA and EDTA, respectively.

Figure 3 shows the FTIR spectra of the ferrite powders after combustion. For all the samples, there are bands at about 547 cm^{-1}, which correspond to the interactions between oxygen ions and metal ions occupying the tetra- and octahedral positions in the spinel crystal lattice. This confirms the earlier results, i.e., the formation of ferrite after gel combustion. When the mixture of citric acid (CA) and EDTA is used as the fuel, additional absorption peaks appear in the FTIR spectra at 3500 cm^{-1}. The bands correspond to the stretching and deformation vibrations of the water molecules. This means that most probably the drying process should be further extended. In the FTIR spectrum one can distinguish vibrations originating from the part of the fuels unreacted during combustion. The vibrations confirm that stable metal complexes form during gelation. Absorption bands ($\nu^{as}_{COO^{-1}}$) at

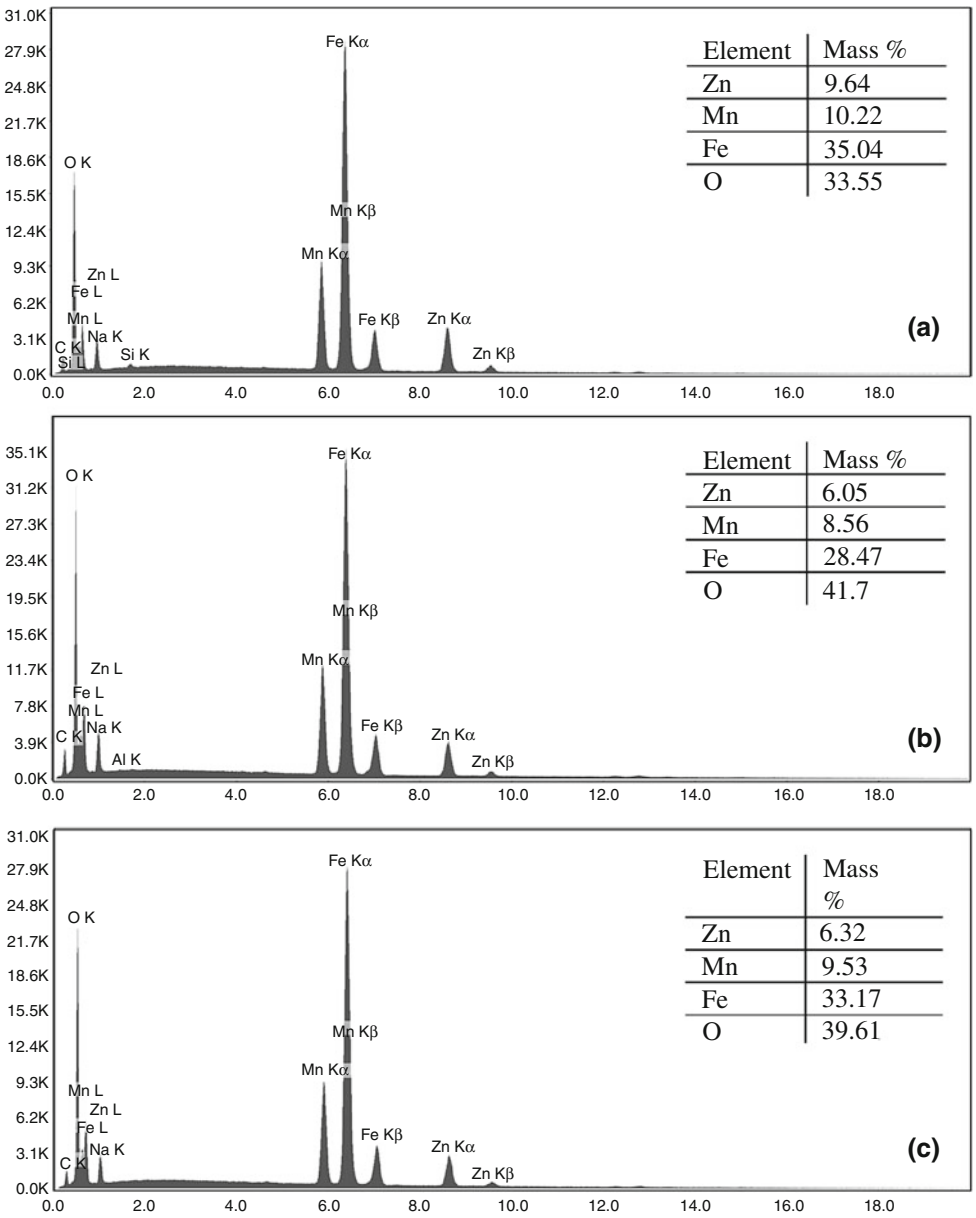

Fig. 7 EDS analysis for ferrite powders prepared from: (**a**) glycine, (**b**) citric acid, and (**c**) citric acid and EDTA

1384 and 1598 cm^{-1} are characteristic of the multidentate type of coordination [25, 31]. When glycine or citric acid is used as the fuel (Fig. 3a, b), the bands are less intensive. No bands originating from water occur for the above samples. FTIR results reveal that only in the case of citric acid the reagents are completely reacted after synthesis. This is confirmed by a TG/DTA analysis of the obtained ferrite powders. Also in the XRD patterns (Fig. 1) there is a well-crystallized spinel phase for the ferrites synthesized from citric acid or glycine. In the case of the fuel mixture, the XRD pattern is less intensive and the elevated background may suggest the presence of an amorphous phase.

The thermal behavior of powders obtained from gel combustion was investigated by TG/DTA heating in a temperature range of 20–1300 °C (Fig. 4). The DTA curve for the ferrite produced using glycine as the fuel (Fig. 4a) features an exothermic peak at a temperature of about 330 °C. The heat treatment process is also accompanied by slight (5 %) mass loss as seen from TG curve. Whereas for the fuel mixture of citric acid and EDTA the exothermic peak at the same temperature is more intensive and the mass loss larger (14 %) (Fig. 4c). The thermal effects observed at these temperatures are connected with the decomposition of the organic residues after the gel combustion. The larger mass loss as depicted on TG curve (Fig. 4c) in the case of the fuel mixture indicates that the combustion process is incomplete, as additionally confirmed by the FTIR spectra (Fig. 3c) and XRD patterns

(Fig. 1c) of the obtained ferrite powders. When the Mn–Zn ferrite is synthesized in the reaction with citric acid as combustion fuel (Fig. 4b), no mass loss on the TG curve attributed to the decomposition of organic residues is observed. In the temperature range of 1100–1200 °C a slight inflection is visible in the DTA curve for the powders obtained from glycine and citric acid. A slight change in mass on the TG curve corresponds to this effect. Angermann et al. [25] suggested that thermodynamically stable Mn–Zn ferrite forms at this temperature. The XRD patterns of the powders after the TG/DTA analysis performed to the temperature of 1300 °C (Fig. 2) reveal a pure spinel phase. Stable, well-crystallized Mn–Zn ferrite forms after high-temperature thermal treatment, regardless of the fuel used earlier.

The microstructure of the obtained materials was examined under a scanning electron microscope (Fig. 5). Because of their magnetic properties, all the materials show a tendency to combine into larger aggregates. The use of glycine as the fuel contributes to the formation of agglomerates (nonuniform in their shape and size) of ferrite powder particles (Fig. 5a), while much larger porous (sponge-like) structures occur beside small aggregates of particles when citric acid or the mixture of CA and EDTA is used (Fig. 5b, c). Such formations can be easily mechanically broken. Figure 6 shows the microstructure (larger magnification; 10000×) of the powders obtained from glycine and from the mixture of CA and EDTA. As shown in Fig. 6a, the Mn–Zn ferrite synthesized from glycine consists of original particles (of several nanometers in size) forming agglomerates which are not very porous. Whereas the powders obtained from the fuel mixture (CA and EDTA), besides the originally synthesized grains, are made up of secondarily sintered particles forming loose porous structures.

EDS measurements (Fig. 7) confirm the presence of Zn, Mn, and Fe in the obtained ferrite powders. An analysis of the compositions of the samples shows a slight difference in the amounts of Zn, Mn, and Fe. Nevertheless, the mutual quantitative ratio of the elements indicates that the composition of the synthesized materials is close to the assumed one ($Mn_{0.6}Zn_{0.4}Fe_2O_4$). The slight disproportions may be due to the possible evaporation of Zn during the synthesis at elevated temperatures [32], and to the formation of a mixture of metastable ferrites after gel combustion.

Conclusions

Phase-pure metastable Mn–Zn ferrites were obtained as a result of low-temperature combustion synthesis from different fuels. The ferrites do not contain foreign nonmagnetic phases (e.g., hematite), as evidenced by the lack of peaks characteristic of such phases in the XRD patterns. The average crystallite size is the smallest (40.0 nm) for the sample obtained from citric acid and EDTA as the fuel. Even the short heating of the powders during the DTA analysis up to 1300 °C results in the transformation of the mixture of the metastable ferrites into a thermodynamically stable form. The use of the mixture of CA and EDTA as the fuel in the synthesis contributes to the formation of powders with a loose sponge-like structure, which is due to the character of the complexes formed during gelation. The use of citric acid (CA) with an additional metal ion-coordinating compound (EDTA in this study) may constitute one of the factors inhibiting the formation of hard agglomerates.

Open Access This article is distributed under the terms of the Creative Commons Attribution License which permits any use, distribution, and reproduction in any medium, provided the original author(s) and the source are credited.

References

1. Hwang C-S, Wang N-C. Preparation and characteristics of ferrite catalysts for reduction of CO_2. Mater Chem Phys. 2004;88:258–63.
2. Klimkiewicz R, Przybylski K, Baran J, Mišta W. Mg–Zn and Mn–Zn ferrites derived from coil core materials as new precursors for catalysts of primary alcohols transformations. Ind Eng Chem Res. 2009;48:6291–5.
3. Winiarska K, Szczygieł I, Klimkiewicz R. Manganese–zinc ferrite synthesis by the sol–gel autocombustion method. Effect of the precursor on the ferrite's catalytic properties. Ind Eng Chem Res. 2013;52:353–61.
4. Kadu AV, Jagtap SV, Chaudhari GN. Studies on the preparation and ethanol gas sensing properties of spinel $Zn_{0.6}Mn_{0.4}Fe_2O_4$ nanomaterials. Curr Appl Phys. 2009;9:1246–51.
5. Giri J, Pradhan P, Somani V, Chelawat H, Chhatre S, Banerjee R, Bahadur D. Synthesis and characterizations of water-based ferrofluids of substituted ferrites [$Fe_{1-x}B_xFe_2O_4$, B = Mn, Co (x = 0–1)] for biomedical applications. J Magn Magn Mater. 2008;320:724–30.
6. Yang C, Jie R, Jianbo L, Yan L. Thermo-responsive Mn–Zn ferrite/poly(*N*,*N*′-isopropyl acrylamide-co-*N*-hydroxymethylacrylamide) core/shell nanocomposites for drug-delivery systems. J Biomat Sci Polym E. 2011;22:1473–86.
7. Le Guével X, Prinz E-M, Müller R, Hempelmann R, Schneider M. Synthesis and characterization of superparamagnetic nanoparticles coated with fluorescent gold nanoclusters. J Nanopart Res. 2012;14:727–36.
8. Hou X, Feng J, Liu X, Ren Y, Fan Z, Zhang M. Magnetic and high rate adsorption properties of porous $Mn_{1-x}Zn_xFe_2O_4$ ($0 \le x \le 0.8$) adsorbents. J Colloid Interf Sci. 2011;353:524–9.
9. Habibi MH, Habibi AH. Effect of the thermal treatment conditions on the formation of zinc ferrite nanocomposite, $ZnFe_2O_4$, by sol–gel method. J Therm Anal Calorim. 2012. doi: 10.1007/s10973-012-2830-4.
10. Arulmurugan R, Vaidyanathan G, Sendhilnathan S, Jeyadevan B. Mn–Zn ferrite nanoparticles for ferrofluid preparation: study on thermal–magnetic properties. J Magn Magn Mater. 2006;298:83–94.
11. Rao BP, Kim CO, Kim C, Dumitru I, Spinu L, Caltun OF. Structural and magnetic characterizations of coprecipitated Ni–Zn and Mn–Zn ferrite nanoparticles. IEEE Trans Magn. 2006;42:2858–60.

12. Dasgupta S, Kim KB, Ellrich J, Eckert J, Manna I. Mechanochemical synthesis and characterization of microstructure and magnetic properties of nanocrystalline $Mn_{1-x}Zn_xFe_2O_4$. J Alloys Compd. 2006;424:13–20.
13. Botta PM, Bercoff PG, Aglietti EF, Bertorello HR, Porto López JM. Two alternative synthesis routes for MnZn ferrites using mechanochemical treatments. Ceram Int. 2006;32:857–63.
14. Rath C, Sahu KK, Anand S, Date SK, Mishra NC, Das RP. Preparation and characterization of nanosize Mn–Zn ferrite. J Magn Magn Mater. 1999;202:77–84.
15. Praveena K, Sadhana K, Bharadwaj S, Murthy SR. Development of nanocrystalline Mn–Zn ferrites for high frequency transformer applications. J Magn Magn Mater. 2009;321:2433–7.
16. Azadmanjiri J. Preparation of Mn–Zn ferrite nanoparticles from chemical sol–gel combustion method and the magnetic properties after sintering. J Non-Cryst Solids. 2007;353:4170–3.
17. Waqas H, Qureshi AH. Influence of pH on nanosized Mn–Zn ferrite synthesized by sol–gel auto combustion process. J Therm Anal Calorim. 2009;98:355–60.
18. Costa ACFM, Silva VJ, Xin CC, Vieira DA, Cornejo DR, Kiminami RHGA. Effect of urea and glycine fuels on the combustion reaction synthesis of Mn–Zn ferrites: evaluation of morphology and magnetic properties. J Alloys Compd. 2010;495:503–5.
19. Szczygiel I, Winiarska K. Low-temperature synthesis and characterization of the Mn–Zn ferrite. J Therm Anal Calorim. 2011;104:577–83.
20. Gonsalves LR, Mojumdar SC, Verenkar VMS. Synthesis and characterization of ultrafine spinel ferrite obtained by precursor combustion technique. J Therm Anal Calorim. 2012;108:859–63.
21. Jiang J, Ai L, Li L-C. Synthesis and magnetic performance of polyaniline/Mn–Zn ferrite nanocomposites with intrinsic conductivity. J Mater Sci. 2009;44:1024–8.
22. Aubery C, Solans C, Sanchez-Dominguez M. Tuning high aqueous phase uptake in nonionic water-in-oil microemulsions for the synthesis of Mn–Zn ferrite nanoparticles: phase behavior, characterization, and nanoparticle synthesis. Langmuir. 2011;27:14005–13.
23. Sastry PU, Sen D, Mazumder S, Chavan SV, Tyagi AK. Fractal behavior of nanocrystalline ceria–yttria solid solution. J Solid State Chem. 2003;176:57–61.
24. Rath C, Anand S, Das RP, Sahu KK, Kulkarni SD, Date SK, Mishra NC. Dependence on cation distribution of particle size, lattice parameter, and magnetic properties in nanosize Mn–Zn ferrite. J Appl Phys. 2002;91:2211–5.
25. Angermann A, Töpfer J, Da Silva KL, Becker KD. Nanocrystalline Mn–Zn ferrites from mixed oxalates: synthesis, stability and magnetic properties. J Alloys Compd. 2010;508:433–9.
26. Feng Q, Ma XH, Yan QZ, Ge CC. Preparation of soft-agglomerated nano-sized ceramic powders by sol–gel combustion process. Mater Sci Eng B. 2009;162:53–8.
27. Xu G, Ma H, Zhong M, Zhou J, Yue Y, He Z. Influence of pH on characteristics of $BaFe_{12}O_{19}$ powder prepared by sol–gel autocombustion. J Magn Magn Mater. 2006;301:383–8.
28. Klug HP, Alexander LE. X-ray diffraction procedures for polycrystalline and amorphous materials. New York: Willey; 1974.
29. Jain SR, Adiga KC, Verneker VRP. A new approach to thermochemical calculations of condensed fuel–oxidizer mixtures. Combust Flame. 1981;40:71–9.
30. Ge L, Zhou W, Ran R, Shao Z, Liu S. Facile autocombustion synthesis of $La_{0.6}Sr_{0.4}Co_{0.2}Fe_{0.8}O_{3-\delta}$ (LSCF) perovskite via a modified complexing sol–gel process with NH_4NO_3 as combustion aid. J Alloys Compd. 2008;450:338–47.
31. Stoia M, Tudoran LB, Barvinschi P. Nanosized zinc and magnesium ferrites obtained from PVA–metal nitrates' solutions. J Therm Anal Calorim. 2013. doi: 10.1007/s10973-012-2888-z.
32. Chen SH, Chang SC, Lin IN, Tung MJ, Shu WB. Effect of sintering parameters on Zn loss for preparation of high permeability MnZn ferrites. IEEE Trans Magn. 1992;28:2436–8.